Exact Reconstruction of THz Sub-λ Source Features in Knife-Edge Measurements

Marco Peccianti, Matteo Clerici, Alessia Pasquazi, Lucia Caspani, Sze Phing Ho, Fabrizio Buccheri, Jalil Ali, Alessandro Busacca, Tsuneyuki Ozaki, and Roberto Morandotti

(Invited Paper)

***Abstract*—The spatial features of a subwavelength terahertz source are not accessible using time-integrated knife-edge (KE) techniques due to the nonseparable space-time nature of the radiated field and to systematic modifications induced by the blade itself. We show that by combining KE with a time-resolved electro-optical sampling, the space-time coupling can be addressed and the source field profile can be exactly reconstructed.**

***Index Terms*—Phase-sensitive field characterization, spatiotemporal field characterization, subwavelength sources, terahertz (THz) sources.**

I. Introduction

TERAHERTZ (THz) imaging has been the subject of intense research efforts in the last few years, owing to the recognized THz spectroscopic capabilities in material analysis [1]–[5]. The long wavelengths associated with THz radiation (100–1000 μm) impose stringent limitations on the spatial resolution achievable exploiting standard imaging systems. For this reason, several near-field techniques have been proposed and successfully implemented after the first demonstrations by Hunsche [6] and Chen *et al.* [7], achieving subwavelength resolution down to the nanometric scale (see, e.g., [8]–[10]). These schemes employ subwavelength apertures, tips, or other spatial discriminators to scan the THz illuminated object and are usually associated with a poor signal-to-noise ratio (SNR)—see, e.g., [11] and [12]. Yuan *et al.* demonstrated that the SNR could be boosted—when generating a THz field spatially localized on deeply subwavelength dimensions—by exploiting the optical rectification from a focalized optical pump [13]. This can be conveniently exploited for an alternative THz imaging scheme, based on a localized generation, illuminating an object placed within the source near-field. An imaging raster-scan approach can then be implemented by steering the optical pump. In this perspective, the investigations on the spatial and spectral properties of a subwavelength THz source and its interaction with the object to be imaged are essential for the realization of an imaging protocol. This issue has been recently addressed, e.g., by spectrally resolving the knife-edge (KE) measurement technique [14]–[16]. However, a subwavelength beam profiling by KE is still the subject of experimental and theoretical investigations since several effects, mainly polarization dependent, concur in deteriorating the quality of the retrieved information [17], [18].

In this paper, we discuss the origin of some inherent aberrations in the KE characterization of subwavelength sources, which appear evident when the full, spatiotemporal electric-field profile is resolved. Specifically, we address the problem of the transmission of an electromagnetic field from a perfectly conducting half-plane with the exact Sommerfeld approach and we show that the KE technique introduces a spatiotemporal aberration of the field under test that affects the source profiling and, to some extent, limits the reliability of certain subwavelength imaging protocols relying on raster scanning.

By exploiting the temporal electric-field resolution associated with THz time-domain spectroscopy (TDS), we theoretically, numerically, and experimentally address the aberration issue and we show how, under a limited set of conditions, such aberration can be eliminated.

The manuscript is organized as follows. Section II addresses the space-time nonseparability characteristic of extremely localized optical fields and its effect on a KE measurement. In Section III, we introduce the basis for a field-resolved KE

The work of M. Peccianti was supported by the Marie Curie People IOF project (TOBIAS PIOF-GA-2008-221262). The work of M. Clerici was supported in part by "Le Fonds qu´eb´ecois de la recherche sur la nature et les technologies" (FQRNT) through the Minist`ere de l' ´Education, du Loisir et du Sports du Qu´ebec (MELS) fellowship program and in part by the IOF People Programme (Marie Curie Actions) of the European Union's FP7-2012, KO-HERENT, GA 299522. The work of L. Caspani was supported in part by "Le Fonds qu´eb´ecois de la recherche sur la nature et les technologies" (FQRNT) through the MELS fellowship program and in part by the Government of Canada through the Post-Doctoral Research Fellowships (PDRF) program. The work of S. P. Ho was supported by Universiti Teknologi Malaysia through the Skim Latihan Akademik IPTA (SLAI) fellowship program. The work of F. Buccheri was supported by "Le Fonds qu´eb´ecois de la recherche sur la nature et les tech-nologies" (FQRNT) through the MELS fellowship program.

M. Peccianti is with the Institute for Complex Systems, National Research Center (CNR), 00185 Rome, Italy (e-mail: m.peccianti@gmail.com).

M. Clerici is with the Ultrafast Optical Processing Group, INRS-EMT, Varennes, QC J3X 1S2, Canada and also with the School of Engineering and Physical Sciences, Heriot-Watt University, Edinburgh EH14 4AS, U.K. (e-mail: clerici@emt.inrs.ca).

A. Pasquazi, L. Caspani, T. Ozaki, and R. Morandotti are with the Ultrafast Optical Processing Group, INRS-EMT, Varennes, QC J3X 1S2, Canada (e-mail: alessia.pasquazi@gmail.com; caspani@emt.inrs.ca; morandott@emt.inrs.ca).

S. P. Ho is with the Ultrafast Optical Processing Group, INRS-EMT, Varennes, QC J3X 1S2, Canada and also with the Nanophotonics Research Alliance, UniversitiTeknologi Malaysia, UTM Skudai, 81310 Johor, Malaysia (e-mail: szephing@emt.inrs.ca).

F. Buccheri is with the Institute of Optics, University of Rochester, NY 14627 USA (e-mail: fbuccheri@yahoo.it).

J. Ali is with the APSI, Universiti Teknologi Malaysia, UTM Skudai, 81310 Johor, Malaysia (e-mail: ali@apsi.com).

A. Busacca is with DIEET, University of Palermo, 61-90133 Palermo, Italy (e-mail: busacca@unipa.it).

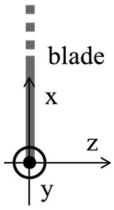

Fig. 1. Reference system: the blade is in the plane $z = 0$ for $x_o > 0$.

measurement and we describe the experimental apparatus employed for the generation and detection of a subwavelength, single-cycle THz wave. We also show the numerical modeling, implemented through a finite-difference time-domain (FDTD) approach, of the KE measurement and the appearance of a space-time aberration in the reconstructed field. In Section IV, we provide some physical insight on the origin of the observed space-time aberration through an exact analytical model. We derive the explicit form of the transfer function of the KE measurement, which allows for the retrieval of the original source profile from the measured one. Finally, we draw the conclusions summarized in Section V. An Appendix follows, where we describe the details of our theoretical model.

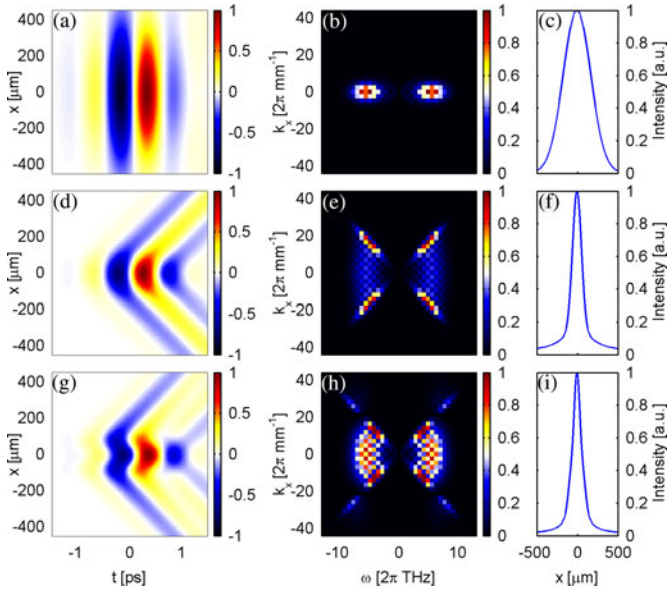

Fig. 2. (a)–(c) Propagation of a superwavelength field: (a) field in space and time, (b) Fourier transform, and (c) intensity profile after the integration in time. (d)–(f) and (g)–(i) are the same as (a)–(c) for two different subwavelength distributions: different space-time profiles share the same intensity-reconstructed profile.

II. Space-Time Coupling in KE Measurements

The KE technique is one of the most-established approaches for the characterization of the spatial profile of optical beams. In the classical implementation, it is based on measuring the optical power transmitted by a blade behaving like a semi-infinite plane, blocking a portion of the optical beam. By repeating the measurement for several transverse positions of the blade in its plane, it is possible to collect the integral of the source optical power along the direction spanned by the blade. Thus, in a large number of cases, the spatial source profile can be retrieved, e.g., by direct differentiation.

This approach is very mature and has the striking advantage to provide an extremely accurate measurement of the beam spatial distribution without the need of cameras. It has also been exploited for the characterization of subwavelength features that cannot be addressed with standard far-field imaging techniques [17].

Let us recall some basic concepts considering the reference system in Fig. 1 for a beam propagating along the z coordinate. The blade is defined in the plane $z = 0$ and covers the optical field on $x_o > 0$. If $I(x, y)$ is the intensity distribution of the optical field in the plane of the blade, the collection of the transmitted power for several positions of the blade edge x_o (varied through small steps dx) operatively implements the operation $\int_{-\infty}^{x_o} \int_{-\infty}^{\infty} I(x, y) dx dy$. This measurement, after a derivative along x, provides the x varying function $\int_{-\infty}^{\infty} I(x_o, y) dy$, i.e., the integral projection of the field intensity along y.

When the intensity can be expressed as the product of two independent functions $I(x, y) = I_x(x) I_y(y)$, i.e., it is *separable* in x and y, the KE along x directly provides the estimation of the x varying component $I_x(x) \int_{-\infty}^{\infty} I_y(y) dy$, and the same consideration can be implemented for the y varying component (see, e.g., [19] and [20]). However, when the field exhibits a nonseparable spatial distribution at the measuring plane, the KE fails to reconstruct the correct beam profile, not accessible in the single integral projection approach. The problem is usually addressed in a tomographic fashion, by cutting the transverse optical distribution with a blade at different angles in the x–y plane.

The temporal dependence of the field under test is usually neglected in standard KE. The method is historically designed to characterize paraxial beams described by a field distribution with a *separable* temporal and spatial dependence.

Several kinds of wavepackets, as for instance those arising from second-order nonlinear interactions, can be featured by the nonseparability of space and time [21], [22]. In such cases, a separate spatial and temporal characterization of the field properties such as coherence [23], [24] and the biphoton probability distribution [25], [26] fails to provide the correct information. We remark that, at a fixed propagation distance z, the time axis t is here considered as the coordinate orthogonal to the transverse plane x–y, in the reference frame comoving with the pulse group velocity.

When nonparaxiality is concerned, such as in the case of extremely localized sources, the field spatial and temporal coordinates are coupled, as can be intuitively understood by considering the space-time profile of a spherical wave. This, in turn, limits the application of the standard KE technique, since the power measurement performed with an energy sensitive slow detector is equivalent to a temporal integration of the intensity distribution.

Fig. 2(a) and (b) shows the spatiotemporal distribution of a paraxial field in x and t (for simplicity we neglect the dependence along y) and its spatiotemporal spectrum in the space of

wavenumbers k_x and angular frequencies *w* (refer to Section IV for the definitions of the Fourier transforms employed here). In this case the field can be factorized into two independent temporal and spatial contributions: the profile of the field intensity along *x*, shown in (c) after integration in time, provides a faithful estimation of the beam spatial distribution. Fig. 2(d), (e) and (g), (h) show a field with the same temporal spectrum of (a, b), but with different subwavelength spatial features. In the Fourier space, it is evident that the components of the field moved toward the straight lines $k_x = \pm\omega/c$. This is simply due to the nature of the Green function of the electromagnetic field that corresponds in the transformed domain to the transfer function

$$\check{G} \propto \frac{1}{\sqrt{(\omega/c)^2 - k_x^2}}. \tag{II.1}$$

Such function possesses a couple of complex conjugate poles on the straight lines $k_x = \pm\omega/c$, where the field is condensed, as it appears for the subwavelength distributions in Fig. 2(e) and (h). Such distributions evidently cannot be factorized into temporal and spatial spectral components (ω and k_x) in the Fourier domain, and consequently, the same holds for the direct domain (*x*, *t*).

As expected, the measurement of the intensity profile after a temporal integration does not provide a proper characterization of the field: while cases (d), (e) and (g), (h) possess a clear different behavior in both space and time, their intensity profile along *x* is the same (f), (i). For a subwavelength distribution is, thus, necessary to address the whole spatiotemporal domain in order to obtain a reliable characterization of the field.

III. THz TDS and KE Characterization: A Space-Time Field-Resolved Approach

As can be inferred from the previous considerations, temporal resolution is essential to address the features of a subwavelength source. When THz is concerned, the commonly adopted detection approach, namely TDS, allows for a direct measurement of the THz electric field resolved in time. A typical example of TDS is the time-resolved electro-optical sampling scheme [27], [28]. A polarized optical probe is overlapped in space to the THz pulse under test in an electro-optical crystal, such as Zinc Telluride (ZnTe). The duration of the THz electric-field oscillations typically exceeds largely those of the probe pulse. Hence, at different THz-optical probe delays, the probe experiences the action of a quasi-static electric field that, through the electro-optical effect enabled by the crystal nonlinearity, translates into a modification of its polarization state. By resolving in time (via different delays) such polarization change, it is thus possible to directly map the THz electric field.

By combining a TDS approach with the KE technique, the characterization of subwavelength THz sources can take advantage of the temporal, field-resolved detection, which is more than what is required by the separability considerations expressed in the previous section.

In its standard form, a time-resolved KE approach would require to measure the total power radiated by the source after the blade clipping [17]. In such a case, the measured quantity is the time-resolved energy (or average power) at different blade positions

$$U(x_0, t) = \int_{-\infty}^{x_o} I(x, t)\, dx \tag{III.1}$$

and the spatiotemporal intensity profile can be readily obtained by a direct derivative of $U(x_0, t)$ with respect to the blade coordinate. However, for subwavelength sources the requirement of collecting the total radiated power poses serious experimental issues.

Conversely, for an electric-field-resolved measurement the most direct way to retrieve the spatiotemporal electric-field profile via KE would be to record a signal that is proportional to the integral of the electric field, rather than the power. In such a case, the KE measurement would read

$$e(x_0, t) \propto \int_{-\infty}^{x_o} e^{(i)}(x, t)\, dx \tag{III.2}$$

where $e^{(i)}(x, t)$ is the THz real-valued electric field under test (incident field) that may be obtained by a direct differentiation of the measured field $e(x_0, t)$.

The electric field in the far-field $z \to \infty$ is proportional to the Fourier transform of the field at the blade plane. Its value at a point $x = 0$ is then proportional to the integral of the field radiated after the blade clipping; formally

$$e(x = 0, z \to \infty, t) \propto \int_{-\infty}^{+\infty} \mathbf{e}(x, z = 0, t)\, dx \tag{III.3}$$

(we again consider only a single spatial dimension for the sake of simplicity). Thus, for an electric-field-resolved KE spatiotemporal imaging, in contrast to the classical intensity resolved case, it is sufficient to record the field at a point in the far-field of the blade plane.

Operatively, the low THz fields emitted by optical rectification on subwavelength areas will require an optical system—with an impulse response $h(x, y)$—that allows performing TDS of a reasonably strong signal.

The field in the reconstruction plane $z = z_{\text{out}}$ then reads:

$$e(x, y, z_{\text{out}}) = \iint_{-\infty}^{\infty} e(\xi, \eta, z = 0)\, h(x - \xi, y - \eta) d\xi d\eta. \tag{III.4}$$

The field in the image plane sampled in the point $x = 0, y = 0$ is, thus, approximated by the integral of the field in the image plane, whenever the size of any spatial feature of interest is much smaller than the system spatial resolution

$$\begin{aligned} e(x = 0, y = 0, z_{\text{out}}) &= \iint_{-\infty}^{\infty} e(\xi, \eta, z = 0)\, h(-\xi, -\eta)\, d\xi d\eta \\ &\approx \iint_{-\infty}^{\infty} e(\xi, \eta, z = 0)\, d\xi d\eta \end{aligned} \tag{III.5}$$

that in our case translates into the requirement of an impulse response function nearly constant over few wavelengths.

For this purpose, we considered an imaging system composed by two off-axis parabolic mirrors of limited aperture. Since both the spatial resolution and the signal at the detection plane are directly proportional to the numerical aperture (NA) of the

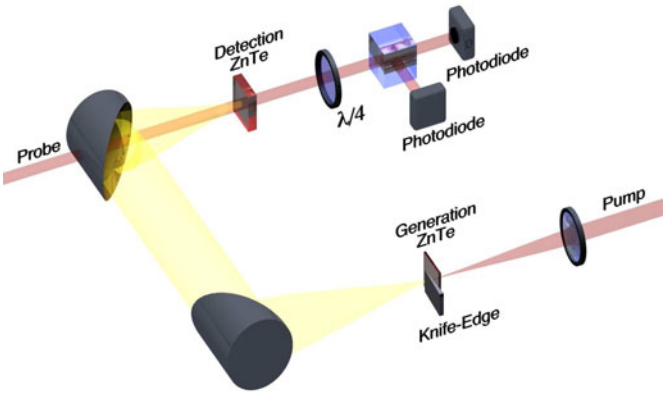

Fig. 3. Sketch of the experimental setup employed for the generation and characterization of the subwavelength THz source.

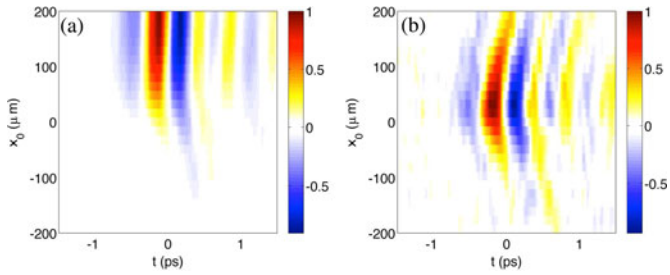

Fig. 4. (a) Electric field measured in the focus of the second parabolic mirror, as a function of the blade position x_o and time. (b) Electric field retrieved by means of spatial differentiation.

imaging system, a tradeoff between a correct implementation of a field-resolved KE (low NA) and a reasonably high SNR in the detection (high NA) has to be found. It has to be noted that the imaged radiation is not monochromatic; hence, the effect of a finite NA also unavoidably translates into a high-pass temporal frequency filter, which accompanies our measurements. Finally, we point out that the broken radial symmetry determined by the vectorial effects accompanying nonparaxial focusing is not accounted for in our investigations [29].

A. *Experimental Setup*

The experimental setup adopted for our study is sketched in Fig. 3. An 800-nm, 100-fs, 5-nJ train of pulses at 80-MHz repetition rate, delivered by a Ti:sapphire ultrafast oscillator (MaiTai, Spectra Physics), is tightly focused by a 5 cm focal lens on a second-order nonlinear crystal. Due to the extreme divergence of the generated subwavelength THz field, the effective source dimension is limited by the crystal thickness. Hence, in order to produce a highly localized THz emission, the optical rectification is excited in a $\langle 1\ 1\ 0\rangle$-oriented, 20-μm-thick (subwavelength for THz) ZnTe crystal, bonded on a 500-μm-thick $\langle 1\ 00\rangle$ ZnTe substrate, which does not contribute to the generation. By varying the pump beam diameter in front of the lens, the effective THz beam waist can be controlled.

For the experiment reported here, the pump beam waist was set to 30 μm, i.e., nearly $\lambda/10$ of the generated THz wavelength (carrier wavelength $\simeq$ 300 μm).

The THz radiation is then partially collimated by a gold-coated, 2-in aperture off-axis parabolic mirror, with a 2-in equivalent focal length, setting the numerical aperture of the diagnostic at NA $\simeq$ 0.45 (compatible with the requirement of field integration on areas with radii $<$ 150 μm). The collimated THz beam is finally focused into the detection crystal by a second parabolic mirror (identical to the first one), featured with a small aperture that allows an optical probe pulse to reach the THz focus. The detection crystal is a 3-mm, $\langle 1\ 1\ 0\rangle$ cut ZnTe, and a standard electro-optical sampling scheme is employed for the THz time-resolved electric-field measurement.

The KE is performed via an aluminum blade directly contacted to the surface of the generation crystal and the time-resolved electric field at the detection focus is then recorded for different blade-edge to optical pump beam distances x_o. Following our previous considerations, due to the limited NA of the imaging system, the TDS implements a time-resolved field-sensitive detection, for any blade position, of the mean field at the blade plane (also the generation plane). The measured field is shown in Fig. 4(a).

By taking the derivative of the measured time-resolved electric field along the blade coordinate, it is then possible to retrieve the spatiotemporal electric-field profile of the source, which is shown in Fig. 4(b): an evident asymmetry along the spatial coordinate appears despite the expected spatial symmetry of the THz source.

B. *Numerical Modeling of the Experimental Setup*

In order to investigate the asymmetry revealed by our experimental findings, we performed a set of numerical simulations with an FDTD numerical solver. We modeled all the main components of the experimental setup: a subwavelength, p-polarized (polarization parallel to the blade edge) THz source; a metallic blade; and the imaging system. The parabolic mirror sizes and foci have been chosen in order to match the NA of the experimental imaging system.

Due to computational constraints, we consider a reduced, 2-D+1 geometry [(x, z)+t]. Although different from a full 3-D+1 case, the results are qualitatively compatible with the prediction of a full 3-D theory (see Section IV).

We modeled the sub-λ source as a pulsed current source term in Maxwell's equations, polarized along y (corresponding to the p-polarization in our experiment), with a carrier wavelength $\lambda = 300$ μm. The current source term has a 50 μm diameter (full width at 1/e) along the x-axis, no extension in the z direction, and a 0.5 ps duration (full width at 1/e).

A 10-μm-thick metallic blade, extended for $x_o > 0$ along the x-axis, was placed in the focus plane of the first parabolic mirror, 25 μm far from the source. We propagate the THz pulse for different blade-edge positions (x_o) and we monitored the electric field in a point in the focal plane of the second parabolic mirror.

The results of our simulations are reported in Fig. 5: panel (a) shows the field in the focus of the second parabolic mirror, while in panel (b) we plot the reconstructed field obtained by

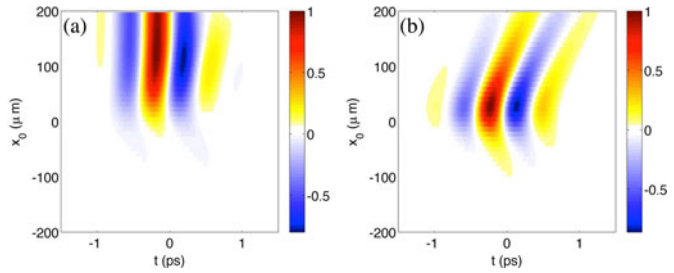

Fig. 5. (a) Electric field in the focus of the second parabolic mirror, evaluated through FDTD numerical simulations. (b) Electric field retrieved by means of calculating the derivative along x_o.

performing the spatial derivative of the field in (a) along the moving blade direction.

The numerical results match qualitatively well the experimental findings, showing a similar asymmetry in the retrieved field. As we will see in the next section, this effect has to be regarded to as inherent to the investigated technique.

In order to better understand the physical origin of this asymmetry, we developed an analytical model describing the interaction between the blade and the subwavelength source.

IV. Theoretical Establishment of Field Reconstruction Through Space-Time KE: A New Transfer Function

We present in this section the analytical derivation of the transfer function of an ideal KE+TDS system for the characterization of the electric field. Under ideal conditions, the blade can be assumed as a perfectly conductive semi-infinite plane, with negligible thickness. In this case, it is possible to find an analytical rigorous solution of the scattered electric field: historically, the scattering of an electromagnetic field by a semi-infinite conductive plane is the first rigorous diffraction problem solved in electromagnetism; the solution was obtained by Sommerfeld in 1896. For the benefit of the reader, we will briefly recall the approach in the Appendix, targeting the specific problem of the reconstruction of THz fields generated by optical rectification. Here, we will directly employ the results for the derivation of the exact equation for the KE+TDS system in the case of a THz field p-polarized to the blade edge (*y* polarized in the geometry depicted in Fig. 1). The case for a general transverse polarization is treated in the Appendix.

Before entering in the details, we define here the conventions on the Fourier transforms adopted in the text: the THz electric field is defined in time *t*/frequency ω by the Fourier relation

$$\mathbf{e}\left(\mathbf{r},t\right)=2\boldsymbol{Re}\int_{-\infty}^{\infty}\mathbf{E}\left(\mathbf{r},\omega\right)e^{-i\omega t}\frac{d\omega}{2\pi} \tag{IV.1}$$

in the $\mathbf{r}$, ω space. Considering z the propagation coordinate, it is useful to define a spatial Fourier transform for the transverse coordinates *x,y* as (we omit here the dependence on ω)

$$\check{\mathbf{E}}\left(k_x,k_y,z\right)=\iint_{-\infty}^{\infty}\mathbf{E}\left(x,y,z\right)e^{-ik_x x-ik_y y}dxdy \tag{IV.2}$$

that is, for the total spatiotemporal field:

$$\mathbf{e}\left(x,y,z,t\right)=2\boldsymbol{Re}\iiint_{-\infty}^{\infty}\check{\mathbf{E}}\left(k_x,k_y,z,\omega\right)e^{ik_x x+ik_y y-i\omega t}\times\frac{dk_x dk_y d\omega}{\left(2\pi\right)^3}. \tag{IV.3}$$

We model the blade as a semi-infinite perfectly conductive plane defined in $z=0$ for $x_o>0$. As discussed previously, the TDS system implements the integral along *x* and *y* of a specific polarization associated with the field transmitted by the blade in the plane $z=0^+$, i.e., for each position of the blade, we collect the quantity $\iint_{-\infty}^{\infty}\mathbf{E}\left(x,y,z=0^+,\omega\right)\cdot\hat{\boldsymbol{u}}dxdy$, where $\hat{\boldsymbol{u}}$ is a versor parallel to the transverse polarization detected by the system. This operation is equivalent to sampling the Fourier transform at zero:

$$\check{\mathbf{E}}\left(k_x=0,k_y=0,z=0^+,\omega\right)\cdot\hat{\boldsymbol{u}}. \tag{IV.4}$$

With a scan along *x* we can then only reconstruct the integral along *y* of the electric field in $z=0$, i.e., in the transformed space $\check{\mathbf{E}}^{(i)}\left(k_x,k_y=0,z=0^+,\omega\right)$. For simplicity, we will omit the dependences on $z=0^+$ and $k_y=0$ in the expressions which will follow.

If we consider a *y*-polarized input field $\mathbf{E}^{(i)}=\mathrm{E}^{(i)}\hat{\boldsymbol{y}}$ and a detection along $\hat{\boldsymbol{u}}=\hat{\boldsymbol{y}}$, the following exact relation between the incident $\mathrm{E}^{(i)}$ and the total integral of the field transmitted by the blade holds

$$\check{\mathrm{E}}(k_x=0,\omega)=\check{\mathrm{E}}^{(i)}\left(k_x=0,\omega\right)-\int_{-\infty}^{\infty}\frac{2i}{s_x}\sqrt{1+\frac{cs_x}{\omega}}\check{\mathrm{E}}^{(i)}\left(s_x,\omega\right)e^{i\,s_x x_0}\frac{ds_x}{2\pi}. \tag{IV.5}$$

Equation (IV.5) is directly obtained by evaluating the total field transmitted by a perfectly conductive half-plane, as can be found in several references (see, e.g., [30]) and reported in detail in the Appendix.

We define a "reconstructed" field $\mathrm{e}_R\left(x_0,t\right)$, function of the blade position coordinate x_0, by differentiating (IV.5) with respect to x_0 and transforming back in the temporal domain. We, thus, obtain

$$\mathrm{e}_R(x_0,t)\propto\boldsymbol{Re}\iint_{-\infty}^{\infty}\sqrt{1+\frac{cs_x}{\omega}}\check{\mathrm{E}}^{(i)}(s_x,\omega)e^{is_x x_0-i\omega t}\frac{ds_x d\omega}{(2\pi)^2}. \tag{IV.6}$$

Equation (IV.6) is formally equal to the Fourier transform (in the position of the blade x_0) of the input function $\check{\mathrm{E}}^{(i)}\left(s_x,\omega\right)$, multiplied by the radical term of (IV.6). Considering that the Fourier transform of a real signal possesses a complex conjugate symmetry and that, by hypothesis, $\check{\mathrm{E}}^{(i)}\left(s_x,\omega\right)$ is the Fourier transform of a real signal, it holds $\check{\mathrm{E}}^{(i)}\left(s_x,\omega\right)=\mathrm{conj}(\check{\mathrm{E}}^{(i)}\left(-s_x,-\omega\right))$. Thus, in order to ensure that $\mathrm{e}_R\left(x_0,t\right)$ is a real function, the radical term in (IV.6) must possess a complex conjugate symmetry as well. It is easy to verify that this holds

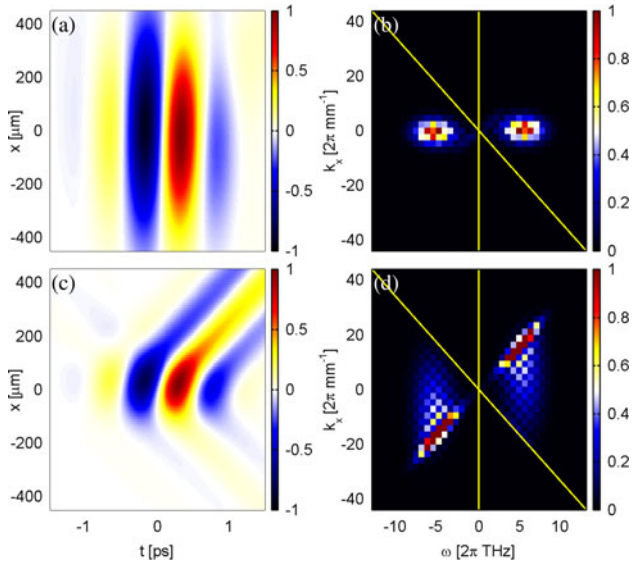

Fig. 6. Effect of the transfer function of the KE+TDS system for a super-wavelength (a), (b) and subwavelength (c), (d) fields in pseudocolor. (a) and (b) Direct and transformed space of the function in Fig. 2(a) and (b) after a multiplication with (IV.8) in the transformed space. The lines indicate the boundaries of the region where (IV.8) is zero. (c) and (d) Same for the subwavelength field in Fig. 2 (e) and (f).

only when it is real; thus, (IV.6) can be rewritten as

$$\mathrm{e}_R\left(x_0,t\right) \propto \iint_{-\infty}^{\infty} H\left(1+\frac{ck_x}{\omega}\right)\sqrt{1+\frac{ck_x}{\omega}}\check{\mathrm{E}}^{(i)} \times\left(k_x,\omega\right)e^{ik_x x_0-i\omega t}\frac{dk_x d\omega}{\left(2\pi\right)^2} \quad \text{(IV.7a)}$$

where H is the Heaviside theta function. Considering the Fourier transform of the reconstructed field, we get

$$\check{\mathrm{E}}^{(R)}\left(k_x,\omega\right) \propto H\left(1+\frac{ck_x}{\omega}\right)\sqrt{1+\frac{ck_x}{\omega}}\check{\mathrm{E}}^{(i)}\left(k_x,\omega\right). \quad \text{(IV.7b)}$$

From (IV.7b), we obtain the transfer function of the KE+TDS system, where we consider explicitly the Heaviside theta function

$$\check{T}\left(k_x,\omega\right) \equiv \begin{cases} \sqrt{1+\dfrac{ck_x}{\omega}}, & \text{for } k_x > -\dfrac{\omega}{c} \\ 0, & \text{for } k_x < -\dfrac{\omega}{c}. \end{cases} \quad \text{(IV.8)}$$

For fields with spatial localization above the wavelength scale, the spectrum is localized in a region where the spatial frequency k_x is small when compared to ω/c, as also visible in the example in Fig. 2(a) and (b). The effect of the transfer function on such fields is negligible as $\check{T}\left(k_x,\omega\right)$ tends to the unit value for small values of ck_x/ω. As heuristically expected, in this case the reconstructed field is proportional to the field under test, as it is clearly visible in Fig. 6(a) and (b) where the distributions proposed in Fig. 2(a) and (b) are multiplied in the transformed space by $\check{T}\left(k_x,\omega\right)$—see (IV.8).

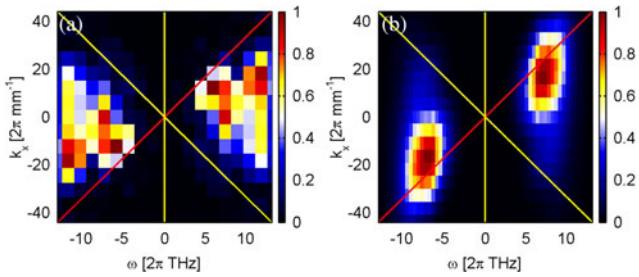

Fig. 7. (a) and (b) Spatiotemporal spectra of the experimental and numerical data in Figs. 4 and 5, respectively. A clear accumulation appears on the straight $k_x = +\omega/c$ (red) and quenching on $k_x = -\omega/c$ (yellow).

Conversely, the transfer function plays a relevant role for sub-wavelength localized fields, filtering out part of the spatiotemporal components of the reconstructed field: $\check{T}\left(k_x,\omega\right)$ is zero for the superluminal components corresponding to the region bounded by the straight lines $k_x = -\omega/c$ and $\omega = 0$. The field reconstructed by the KE+TDS system then undergoes an asymmetric quenching of the spatiotemporal spectrum that translates into an asymmetric distribution in the direct space. This effect is shown in Fig. 6(c) and (d) where $\check{T}\left(k_x,\omega\right)$ is applied to the subwavelength distribution in the example of Fig. 2(d) and (e).

The asymmetric filtering effect can be now clearly recognized in the experimental and numerical results: their Fourier transforms, reported in Fig. 7(a) and (b), respectively, possess components with low energy in the subluminal region where $\check{T}\left(k_x,\omega\right)$ is zero.

From this analysis, it is clear that the KE+TDS system can provide a measurement of the field under test only in the portion of the spatiotemporal spectrum where (IV.8) is significant. However, when it is possible to guess a spatial symmetry in the field under test, this information is sufficient for the full reconstruction of the field. As the symmetry in the direct space corresponds to symmetry in the transformed space, the missing components of the field for $k_x < -\omega/c$ are equal to the components for $k_x > \omega/c$ available in the measurement.

Moreover, if the KE is implemented for negative x_o (i.e., the blade acts for $x_o < 0$), its transfer function becomes

$$\check{T}_{-}\left(k_x,\omega\right) \equiv \begin{cases} -\sqrt{1-\dfrac{ck_x}{\omega}} & \text{for } k_x > \dfrac{\omega}{c} \\ 0 & \text{for } k_x < \dfrac{\omega}{c}. \end{cases} \quad \text{(IV.9)}$$

Remarkably, $\check{T}_{-}\left(k_x,\omega\right)$ is significant where (IV.8) is zero. In turn, a generic subwavelength field can be completely reconstructed when two different KE measurements are performed for positive and negative x_o. In this case, the investigated field in the Fourier domain can be determined with the aid of the two functions

$$\check{\mathrm{E}}_{\pm}^{(i)}\left(k_x,\omega\right) \propto \pm H\left(1\pm\frac{ck_x}{\omega}\right)\sqrt{\frac{\omega}{\omega\pm ck_x}}\check{\mathrm{E}}_{\pm}^{(R)}\left(k_x,\omega\right). \quad \text{(IV.10)}$$

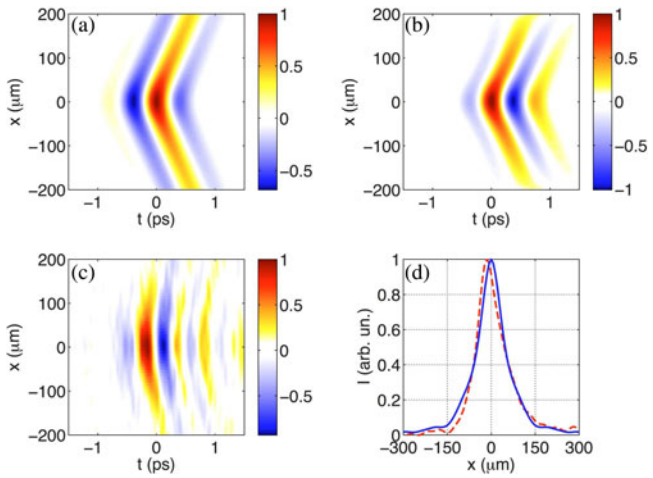

Fig. 8. Results from the data inversion considering the transfer function *T*. (a) Initial spatiotemporal field simulated via FDTD. (b) Retrieved field obtained via KE+TDS: under the hypothesis of a symmetric geometry. (c) Retrieved experimental field profile under the same conditions. (d) Comparison between the beam profile obtained by (blue, solid) and without (red, dashed) taking into consideration the effect of the asymmetric KE transfer function.

In the next section, we show the results obtained by exploiting the developed inversion method on the experimental and numerical data shown in Figs. 4 and 5.

A. Numerical and Experimental Data Inversion

In order to retrieve the spatiotemporal field profile from the numerical and experimental data, we proceeded by dividing the spatiotemporal spectra by the KE transfer function *T*. After that, under the assumption of a symmetric source we recovered the missing information by imposing the spectral-spatial symmetry ($k_x \rightarrow -\mathrm{k}_x$). Considering the source shown in Fig. 8(a), and by applying the method described before on the simulated KE+TDS measurements (see Fig. 5), we retrieved the field shown in Fig. 8(b), thus confirming the validity of the proposed method. On the other hand, we note the appearance of a temporal phase shift of on the reconstructed *x–t* field that may be interpreted as a consequence of the *Gouy* phase shift, as recently commented by Yi *et al.* for subwavelength localized sources [31].

Finally, we performed the same analysis on the experimental data shown in Fig. 4. The retrieved spatiotemporal field profile is presented in Fig. 8(c), while in panel (d) we compare the time-integrated spatial beam profile obtained by evaluating the intensity of the retrieved field (blue) with the same quantity determined by the direct integration of the field in Fig. 4(b), i.e., before the inversion through the *T*-function.

V. Conclusion

This study reports on our recent studies related to the characterization of subwavelength THz sources, the main ingredient for an aperture-free THz near-field imaging. Starting from the consideration that extremely diffractive waves, e.g., non-paraxial, are featured by space-time coupling, we discussed the validity of the standard KE-based approach for a proper beam profiling. Exploiting the unique electric-field time-resolved capabilities offered by THz TDS, we thus investigated experimentally and numerically a field-resolved spatiotemporal characterization technique relying on the combination of KE and electro-optical sampling. We pointed out a systematic error affecting this field-resolved approach and, resorting to the exact Sommerfeld formulation of the scattering problem from an infinite, conducting half-plane, we provided a simple solution for retrieving the full spatiotemporal structure of the sampled field.

As a closing remark, we stress that the proposed investigation is propaedeutic for properly addressing the issues related to raster-scan imaging of subwavelength structures, where systematic aberrations may arise as a consequence of an asymmetric transfer function, similarly to what presented here for a metallic blade.

Appendix

A. Definition of the Vector Potential Equations for the KE

We will treat the diffraction problem from a half-plane and define the polarization-dependent transfer function of the KE with the aid of the vector potential $\mathbf{A}$.

In the ($\mathbf{r}$, ω) space, $\mathbf{A}$ is defined by the relations with the electric field

$$\mathbf{E} = \frac{1}{i\omega\varepsilon_0}\left(\boldsymbol{\nabla}\boldsymbol{\nabla}\cdot\mathbf{A} + k_0^2\mathbf{A}\right) \tag{A1}$$

where ε_0 is the vacuum dielectric constant and $k_o = \omega/c$ is the wavenumber in vacuum. The THz field is generated by optical rectification under the hypothesis of weak generation, i.e., the pump is not depleted/ modified by the generation itself. In this case, the optical field acts as a pure source for the THz field, proportional to a current source $\mathbf{J}^{(i)}$ (defined in the space $z < 0$) by way of the nonlinear second-order tensor. Using the definition in (A1), the vector potential satisfies the wave equation

$$\boldsymbol{\nabla}^2\mathbf{A} + k_0^2\mathbf{A} = \mathbf{J}. \tag{A2}$$

It is important to note that the vector potential $\mathbf{A}$ is always parallel to the current source. As it physically represents the optical field, that is paraxial along the propagation coordinate z, neither the current $\mathbf{J}^{(i)}$ nor the vector potential $\mathbf{A}^{(i)}$ possess longitudinal components along z. Moreover, if the optical beam is $x(y)$ polarized, we obtain a vector potential that is $x(y)$ polarized.

As discussed previously, the quantity under test is $\check{\mathbf{E}}^{(i)}\left(k_x, k_y = 0, z = 0, \omega\right)$. We can express this quantity in function of the spatial Fourier transform $\check{\mathbf{A}}^{(i)}\left(k_x, k_y, z = 0\right)$ of the vector potential in the plane of the blade, $z = 0$. For $z > 0$ we have

$$\mathbf{A}\left(x, y, z\right) = \int \check{\mathbf{A}}\left(k_x, k_y, z = 0\right) e^{ik_x x + ik_y y + i|z|\sqrt{k_0^2 - k_x^2 - k_y^2}} \frac{dk_x dk_y}{\left(2\pi\right)^2}. \tag{A3}$$

Substituting into (IV.4) for $z = 0^+$ and $k_y = 0$ (we will omit this dependence for simplicity), we obtain

$$\begin{bmatrix} \check{E}_x^{(i)}(k_x,\omega) \\ \check{E}_y^{(i)}(k_x,\omega) \\ \check{E}_z^{(i)}(k_x,\omega) \end{bmatrix} = \frac{1}{i\omega\varepsilon_0} \begin{bmatrix} \left(k_0^2 - k_x^2\right) \check{A}_x^{(i)}(k_x,\omega) \\ k_0^2 \check{A}_y^{(i)}(k_x,\omega) \\ -k_x\sqrt{k_0^2 - k_x^2}\, \check{A}_x^{(i)}(k_x,\omega) \end{bmatrix}. \tag{A4}$$

Note that if we have a *y*-polarized source, the field on the blade will be *y*-polarized; conversely, for an *x*-polarized source the field will have a zero *y* component.

If we can reconstruct $\check{\mathbf{A}}^{(i)}(k_x,\omega)$, (A4) will then provide the electric field $\check{\mathbf{E}}^{(i)}(k_x,\omega)$.

We now take into account the quantity measured by the TDS system (IV.4) and substitute into (A1). Considering that $\mathbf{A}$ does not have longitudinal components, we obtain

$$\begin{aligned} &\check{\mathbf{E}}\left(k_x = 0, k_y = 0, z = 0^+\right) \cdot \hat{\boldsymbol{u}} \\ &\qquad = -i\omega\eta_0 \check{\mathbf{A}}\left(k_x = 0, k_y = 0, z = 0^+\right) \cdot \hat{\boldsymbol{u}}. \end{aligned} \tag{A5}$$

As discussed in the next sections, the integral of the total vector potential at the output of the blade $z = 0^+$ is

$$\begin{aligned} &\check{\mathbf{A}}\left(k_x, = 0, k_y = 0, z = 0^+\right) \cdot \hat{\boldsymbol{u}} \\ &= \mathbf{A}^{(i)}\left(k_x = 0, k_y = 0, z = 0^+\right) \cdot \hat{\boldsymbol{u}} \\ &\quad - \int \frac{2i}{s_x}\sqrt{1 + \frac{cs_x}{\omega}} \check{\mathbf{A}}^{(i)}\left(s_x, k_y = 0, z = 0^+\right) \cdot \hat{\boldsymbol{u}} e^{is_x x_0} \frac{ds_x}{2\pi}. \end{aligned} \tag{A6}$$

We can substitute (A6) into (A5), and differentiate for x_0 and transform back in time, as done for (IV.6). This yields

$$\begin{aligned} \mathbf{e}_R(x_0,t) \propto \boldsymbol{Re} \iint_{-\infty}^{\infty} &-i\omega\eta_0 \sqrt{1 + \frac{csk_x}{\omega}} \check{\mathbf{A}}^{(i)} \\ &\times (k_x,\omega)\, e^{is_x x_0 - i\omega t} \frac{dk_x d\omega}{(2\pi)^2}. \end{aligned} \tag{A7}$$

Following the same considerations applied previously on the radical function, and addressing two different KE measurements for positive and negative x_o, we can reconstruct the two functions

$$\check{\mathbf{A}}_{\pm}^{(i)}(k_x,\omega) \cdot \hat{\boldsymbol{u}} \propto \pm H\left(1 \pm \frac{ck_x}{\omega}\right) \sqrt{\frac{\omega}{\omega \pm ck_x}} \frac{\check{\mathbf{E}}_{\pm}^{(R)}(k_x,\omega)}{-i\omega\eta_0} \cdot \hat{\boldsymbol{u}}. \tag{A8}$$

If we now distinguish the two polarizations *x* and *y*, considering (A4) we obtain

$$\begin{bmatrix} \check{E}_{x,\pm}^{(i)}(k_x,\omega) \\ \check{E}_{y,\pm}^{(i)}(k_x,\omega) \\ \check{E}_{z,\pm}^{(i)}(k_x,\omega) \end{bmatrix} \propto \begin{bmatrix} \left(1 - \left(\frac{ck_x}{\omega}\right)^2\right) H\left(1 \pm \frac{ck_x}{\omega}\right) \sqrt{\frac{\omega}{\omega \pm ck_x}} \check{\mathrm{E}}_{x,\pm}^{(R)}(k_x,\omega) \\ H\left(1 \pm \frac{ck_x}{\omega}\right) \sqrt{\frac{\omega}{\omega \pm ck_x}} \check{\mathrm{E}}_{y,\pm}^{(R)}(k_x,\omega) \\ -\frac{ck_x}{\omega}\sqrt{1 - \left(\frac{ck_x}{\omega}\right)^2} H\left(1 \pm \frac{ck_x}{\omega}\right) \sqrt{\frac{\omega}{\omega \pm ck_x}} \check{\mathrm{E}}_{x,\pm}^{(R)}(k_x,\omega) \end{bmatrix}. \tag{A9}$$

Equation (A9) generalizes (IV.10) for both polarizations.

In the next sections, we will treat the problem of the scattering of an electric field by a perfectly conductive half-plane and we shall derive the relations in (IV.4) and (A6), employed in the paper for finding the transfer function of the KE+TDS system.

B. Definition of the Scattering Problem for the Vector Potential

We model the blade as a semi-infinite perfectly conductive plane at $z = 0$ for $x_o > 0$. The total field $\mathbf{E}$ is considered as the superposition of an incident field $\mathbf{E}^{(i)}$ and a scattered field $\mathbf{E}^{(s)}$, generated, respectively, by the input source $\mathbf{J}^{(i)}$ in the free space and by an induced current $\mathbf{J}^{(s)}$on the metallic plane. In particular, the tangential component of the total field E on the metallic plane is zero. As discussed previously, since the optical source is transversely polarized with respect to the metallic plane we consider the input source parallel to the half-plane. For the vector potential, the following relation holds:

$$A_z^{(i)} = A_z^{(s)} = 0. \tag{B1}$$

We now look for the requirements associated with the vector potential in order to satisfy the following condition on the half-plane:

$$\mathbf{E}_{\parallel}^{(i)} + \mathbf{E}_{\parallel}^{(s)} = 0 \text{ for } z = 0 \text{ and } x > x_0. \tag{B2}$$

Using the relation on the electric field in (A1), and (B1) and (B2) for the vector potential, we have

$$\begin{bmatrix} \partial_{xx} + k_0^2 & \partial_{xy} \\ \partial_{xy} & \partial_{yy} + k_0^2 \end{bmatrix} \left(\mathbf{A}^{(i)} + \mathbf{A}^{(s)}\right) = \mathbf{0}. \tag{B3}$$

Since the operator acting on the vector potential is linear, the condition in (B3) implies that

$$\mathbf{A}^{(s)}(x,y,0) = -\mathbf{A}^{(i)}(x,y,0) + \mathbf{A}_{\mathrm{o}}^{(s)} \text{ for } x > x_0 \tag{B4}$$

where $\mathbf{A}_{\mathrm{o}}^{(s)}$ is the solution to the equation

$$\begin{bmatrix} \partial_{xx} + k_0^2 & \partial_{xy} \\ \partial_{xy} & \partial_{yy} + k_0^2 \end{bmatrix} \mathbf{A}_{\mathrm{o}}^{(s)} = \mathbf{0} \tag{B5}$$

valid on the plane of the blade $z = 0$. We now calculate the operator in the transformed wavevectors Fourier space

$\mathbf{k} = (k_x, k_y, k_z)$ of the spatial coordinate $\mathbf{r} = (x,y,z)$, that is

$$\begin{bmatrix} -k_x^2 + k_0^2 & -k_x k_y \\ -k_{xy} & -k_y^2 + k_0^2 \end{bmatrix}. \tag{B6}$$

The determinant of this operator is zero when

$$k_x^2 + k_y^2 = k_0^2 \tag{B7}$$

i.e., $\mathbf{A}_{\mathrm{o}}^{(s)}$ is a field that propagates parallel to the blade. As we are not interested in these components, we can consider $\mathbf{A}_{\mathrm{o}}^{(s)} = 0$. Hence, the relation in (B2) can be rewritten as

$$\mathbf{A}^{(s)}(x,y,0) = -\mathbf{A}^{(i)}(x,y,0) \text{ for } x > x_0. \tag{B8}$$

C. Solution for the Driven Wave Equation for the Potential

The scattered field is generated by a 2-D spatial current distribution on the plane $z = 0$:

$$\mathbf{J}(\mathbf{r}) = \mathbf{J}^{(s)}(x,y)\, 2\pi\delta(z). \tag{C1}$$

Equivalently, in the 2-D transformed space it holds

$$\mathbf{J}^{(s)}(x,y) = \int \check{\mathbf{J}}^{(s)}(k_x,k_y)\, e^{ik_x x + ik_y y} \frac{dk_x dk_y}{(2\pi)^2}. \tag{C2}$$

Substituting (C2) into (A1), we obtain the solution for the scattered electromagnetic potential

$$\mathbf{A}^{(s)}(x,y,z) = -\frac{i}{2}\int \frac{\check{\mathbf{J}}_o^{(s)}(k_x,k_y)}{\sqrt{k_0^2 - k_x^2 - k_y^2}} e^{ik_x x + ik_y y + i|z|\sqrt{k_0^2 - k_x^2 - k_y^2}} \frac{dk_x dk_y}{(2\pi)^2} \tag{C3}$$

or equivalently, we obtain that the Fourier transform on the section $z = 0^+$ of the scattered field is

$$\check{\mathbf{A}}^{(s)}\left(k_x,k_y,z=0^+\right) = -\frac{i}{2}\frac{\check{\mathbf{J}}_o^{(s)}(k_x,k_y)}{\sqrt{k_0^2 - k_x^2 - k_y^2}}. \tag{C4}$$

D. Scattering Current Induced by a Plane Wave

The scattering problem in (B9) is valid only for $x > x_0$. Hence, we can rewrite the identity in terms of a function that coincides with the opposite incident field on the blade, but is an arbitrary function $\mathbf{f}(x,y)$ for $x < x_0$. With the help of the Heaviside theta function $H(x)$, we define (in the direct and the transformed space)

$$\mathbf{C}(x,y) = -\mathbf{A}^{(i)}(x,y,0)\, H(x - x_0) + (1 - H(x - x_0))\, \mathbf{f}(x,y) \tag{D1a}$$

$$\check{\mathbf{C}}(k_x,k_y) = \pi\left[\check{\mathbf{f}}(k_x,k_y) - \check{\mathbf{A}}^{(i)}(k_x,k_y,z=0)\right] + \left[\check{\mathbf{f}}(k_x,k_y) + \check{\mathbf{A}}^{(i)}(k_x,k_y,z=0)\right] \otimes \left(\frac{i}{k_x} e^{-ik_x x_0}\right) \tag{D1b}$$

where the symbol $\otimes$ stands for the convolution with respect to k_x. Substituting (C3) into (B9) for $z = 0$, we have

$$-\frac{i}{2}\iint \frac{\check{\mathbf{J}}^{(s)}(k_x,k_y)}{\sqrt{k_o^2 - k_x^2 - k_y^2}} e^{ik_x x + ik_y y} \frac{dk_x dk_y}{(2\pi)^2} = \iint \check{\mathbf{C}}(k_x,k_y) e^{ik_x x + ik_y y} \frac{dk_x dk_y}{(2\pi)^2} = 0 \quad \text{for } x > x_0. \tag{D2}$$

The solution of (D2) must account for the fact that the current is zero where the blade is not present

$$\int \mathrm{e}^{ik_y y} \frac{dk_y}{2\pi} \int \check{\mathbf{J}}^{(s)}(k_x,k_y)\, e^{ik_x x} \frac{dk_x}{2\pi} = 0. \tag{D3}$$

To solve the integral problem in (D2) and (D3) for the scattering current $\check{\mathbf{J}}^{(s)}(k_x,k_y)$, we introduce a support function $\check{\mathbf{J}}_o^{(s)}(k_x,k_y,s_x)$ defined as

$$\check{\mathbf{J}}^{(s)}(k_x,k_y) = \int \check{\mathbf{J}}_o^{(s)}(k_x,k_y,s_x)\, e^{-ik_x x_0} \frac{ds_x}{2\pi}. \tag{D4}$$

As long as the term in (D4) converges, the condition in (D3) can be simplified in

$$\int \check{\mathbf{J}}_o^{(s)}(k_x,k_y,s_x) e^{[ik_x(x - x_0)]} \frac{dk_x}{2\pi} = 0 \text{ for } x < x_0 \;\; \forall k_y, \forall k s_x. \tag{D5}$$

We can look for a function $\check{\mathbf{J}}_o^{(s)}(k_x,k_y,s_x)$ that satisfies the conditions necessary to apply Jordan's lemma in k_x $\forall k_y, \forall k s_x$ and that has no poles in the complex lower half-plane $\mathrm{im}(k_x) < 0$: in this case, the condition in (D5) is verified.

If we now impose $\check{\mathbf{f}}(k_x,k_y) = \check{\mathbf{A}}^{(i)}(k_x,k_y,z=0)$, we obtain that $\mathbf{C}(x,y)$ is also related to the input field $\check{\mathbf{A}}^{(i)}(k_x, k_y, z=0)$ through an integral relation

$$\check{\mathbf{C}}(k_x,k_y) = \check{\mathbf{A}}^{(i)}(k_x,k_y,z=0) * \left(\frac{2i}{k_x} e^{-ik_x x_0}\right) = 2ie^{-ik_x x_0} \int \frac{\check{\mathbf{A}}^{(i)}(s_x,k_y,z=0)}{k_x - s_x} e^{is_x x_0} \frac{ds_x}{2\pi}. \tag{D6}$$

Substituting (D6) into (D2), the problem simplifies to

$$\int \left[\frac{\check{\mathbf{J}}_o^{(s)}(k_x,k_y,s_x)}{\sqrt{k_o^2 - k_x^2 - k_y^2}} + 4\frac{\check{\mathbf{A}}^{(i)}(s_x,k_y,z=0)}{k_x - s_x} e^{is_x x_0}\right] * e^{[ik_x(x - x_0)]} \frac{dk_x}{2\pi} = 0, x > x_0, \quad \forall k_y, \forall k s_x. \tag{D7}$$

Since $\check{\mathbf{A}}^{(i)}(s_x,k_y,z=0)$ is a constant in the integral, (D7) and (D5) represent the problem of the scattering of a single plane wave by the conductive half-plane.

To solve (D7), we could simply require

$$\check{\mathbf{J}}_o^{(s)}(k_x,k_y,s_x) = -4\check{\mathbf{A}}^{(i)}(s_x,k_y,z=0) * e^{is_x x_0} \frac{\sqrt{k_o^2 - k_x^2 - k_y^2}}{k_x - s_x}.$$

However, we note that the function would not satisfy Jordan's Lemma, as it is not zero for $|k_x| \to \infty$, and would not satisfy (D5). We also note that the term $1/\sqrt{k_o^2 - k_x^2 - k_y^2}$

in the integral gives rise to a couple of complex conjugate poles $k_x = \pm\sqrt{k_o^2 - k_y^2}$, and only the pole $k_x = \sqrt{k_o^2 - k_y^2}$ falls in the upper complex plane, being thus relevant for the integration with Jordan's lemma. Then, also the following relation satisfies the condition in (D7):

$$\check{\mathbf{J}}_o^{(s)}(k_x, k_y, s_x) = -4\,\check{\mathbf{A}}^{(i)}(s_x, k_y, z=0)\, e^{is_x x_0} * \frac{\sqrt{\sqrt{k_o^2 - k_y^2} - k_x}\sqrt{\sqrt{k_o^2 - k_y^2} + s_x}}{k_x - s_x}. \quad \text{(D8)}$$

Since (C8) has only a pole in the upper complex plane, it also satisfies (D5).

E. Total Diffracted Field

Summarizing the previous results, the Fourier transform of the field in the section of the blade $z = 0^+$ is such that

$$\check{\mathbf{A}}\left(k_x, k_y, z=0^+\right) = \mathbf{A}^{(i)}\left(k_x, k_y, z=0^+\right) + \mathbf{A}^{(s)}\left(k_x, k_y, z=0^+\right). \quad \text{(E1)}$$

Using (C4) and (C8) into (B4), we obtain

$$\check{\mathbf{A}}^{(s)}(k_x, k_y, z=0^+) = 2i \int \check{\mathbf{A}}^{(i)}(s_x, k_y, z=0^+) * \frac{\sqrt{\sqrt{k_o^2 - k_y^2} + s_x}}{\sqrt{\sqrt{k_o^2 - k_y^2} + k_x}} \frac{e^{[i(s_x - k_x)x_0]}}{(k_x - s_x)} \frac{ds_x}{2\pi}. \quad \text{(E2)}$$

By substituting (E2) into (E1), the total field can be propagated using (A3) for $z > 0$. By letting $k_x = 0$ and $k_y = 0$, we finally obtain (A6).

REFERENCES

[1] B. B. Hu and M. C. Nuss, "Imaging with terahertz waves," *Opt. Lett.*, vol. 20, no. 16, pp. 1716–1718, 1995.

[2] Q. Wu, T. Hewitt, and X.-C. Zhang, "Two-dimensional electro-optic imaging of THz beams," *Appl. Phys. Lett.*, vol. 69, no. 8, pp. 1026–1028, 1996.

[3] W. L. Chan, J. Deibel, and D. M. Mittleman, "Imaging with terahertz radiation," *Rep. Prog. Phys.*, vol. 70, no. 8, pp. 1325–1379, 2007.

[4] D. T. Petkie, C. Casto, F. C. D. Lucia, S. R. Murrill, B. Redman, R. L. Espinola, C. C. Franck, E. L. Jacobs, S. T. Griffin, C. E. Halford, J. Reynolds, S. O'Brien, and D. Tofsted, "Active and passive imaging in the THz spectral region: phenomenology, dynamic range, modes, and illumination," *J. Opt. Soc. Amer. B*, vol. 25, no. 9, pp. 1523–1531, 2008.

[5] C. Jansen, S. Wietzke, O. Peters, M. Scheller, N. Vieweg, M. Salhi, N. Krumbholz, C. Jördens, T. Hochrein, and M. Koch, "Terahertz imaging: Applications and perspectives," *Appl. Opt.*, vol. 49, no. 19, pp. E48–E57, 2010.

[6] S. Hunsche, "THz near-field imaging," *Opt. Commun.*, vol. 150, no. 1–6, pp. 22–26, 1998.

[7] Q. Chen, Z. Jiang, G. X. Xu, and X. C. Zhang, "Near-field terahertz imaging with a dynamic aperture," *Opt. Lett.*, vol. 25, no. 15, pp. 1122–1124, 2000.

[8] J. F. Federici, O. Mitrofanov, M. Lee, J. W. P. Hsu, I. Brener, R. Harel, J. D. Wynn, L. N. Pfeiffer and K. W. West, "Terahertz near-field imaging," *Phys. Med. Biol.*, vol. 47, no. 21, pp. 3727–3734, 2002.

[9] H.-T. Chen, R. Kersting, and G. C. Cho, "Terahertz imaging with nanometer resolution," *Appl. Phys. Lett.*, vol. 83, no. 15, pp. 3009–3011, 2003.

[10] K. Moon, E. Jung, M. Lim, and Y. Do, "Terahertz near-field microscope: Analysis and measurements of scattering signals," *IEEE Trans. Terahertz Sci. Technol.*, vol. 1, no. 1, pp. 164–168, Sep. 2011.

[11] H. Bethe, "Theory of diffraction by small holes," *Phys. Rev.*, vol. 66, no. 7–8, pp. 163–182, 1944.

[12] F. J. Garcia-Vidal, T. W. Ebbesen, and L. Kuipers, "Light passing through subwavelength apertures," *Rev. Mod. Phys.*, vol. 82, no. 1, pp. 729–787, 2010.

[13] T. Yuan, J. Xu, and X. C. Zhang, "Development of terahertz wave microscopes," *Infrared Phys. Technol.*, vol. 45, no. 5–6, pp. 417–425, 2004.

[14] H. Lin, C. Fumeaux, B. M. Fischer, and D. Abbott, "Modelling of subwavelength THz sources as Gaussian apertures," *Opt. Express*, vol. 18, no. 17, pp. 17672–17683, 2010.

[15] F. Buccheri, M. Peccianti, A. Busacca, T. Ozaki, and R. Morandotti, "Spatial and spectral properties of small area THz generation for subwavelength microscopy," in *Proc. 35th Int. Conf. Infrared Millimeter and Terahertz Waves*, Sep. 2010, pp. 1–2.

[16] H. Lin, C. Fumeaux, B. Seam Yu Ung, and D. Abbott, "Comprehensive modeling of THz microscope with a sub-wavelength source," *Opt. Express*, vol. 19, no. 6, pp. 5327–5338, 2011.

[17] A. H. Firester, M. E. Heller, and P. Sheng, "Knife-edge scanning measurements of subwavelength focused light beams," *Appl. Opt.*, vol. 16, no. 7, pp. 1971–1974, 1977.

[18] P. Marchenko, S. Orlov, C. Huber, P. Banzer, S. Quabis, U. Peschel, and G. Leuchs, "Interaction of highly focused vector beams with a metal knife-edge," *Opt. Express*, vol. 19, no. 8, pp. 7244–7261, 2011.

[19] R. M. O'Connell and R. A. Vogel, "Abel inversion of knife-edge data from radially symmetric pulsed laser beams," *Appl. Opt.*, vol. 26, no. 13, pp. 2528–2532, 1987.

[20] M. A. C. De Araújo, R. Silva, E. De Lima, D. P. Pereira, and P. C. De Oliveira, "Measurement of Gaussian laser beam radius using the knife-edge technique: improvement on data analysis," *Appl. Opt.*, vol. 48, no. 2, pp. 393–396, 2009.

[21] P. Di Trapani, G. Valiulis, A. Piskarskas, O. Jedrkiewicz, J. Trull, C. Conti, and S. Trillo, "Spontaneously generated X-shaped light bullets," *Phys. Rev. Lett.*, vol. 91, no. 9, pp. 93904-1–93904-4, 2003.

[22] O. Jedrkiewicz, M. Clerici, E. Rubino, and P. Di Trapani, "Generation and control of phase-locked conical wave packets in type-I seeded optical parametric amplification," *Phys. Rev. A*, vol. 80, no. 3, p. 033813, 2009.

[23] O. Jedrkiewicz, A. Picozzi, M. Clerici, D. Faccio, and P. Di Trapani, "Emergence of X-shaped spatiotemporal coherence in optical waves," *Phys. Rev. Lett.*, vol. 97, no. 24, p. 243903, 2006.

[24] O. Jedrkiewicz, M. Clerici, A. Picozzi, D. Faccio, and P. Di Trapani, "X-shaped space-time coherence in optical parametric generation," *Phys. Rev. A*, vol. 76, no. 3, p. 033823, 2007.

[25] A. Gatti, E. Brambilla, L. Caspani, O. Jedrkiewicz, and L. Lugiato, "X entanglement: The nonfactorable spatiotemporal structure of biphoton correlation," *Phys. Rev. Lett.*, vol. 102, no. 22, p. 223601, 2009.

[26] L. Caspani, E. Brambilla, and A. Gatti, "Tailoring the spatiotemporal structure of biphoton entanglement in type-I parametric down-conversion," *Phys. Rev. A*, vol. 81, no. 3, p. 033808, 2010.

[27] Q. Wu and X.-C. Zhang, "Free-space electro-optic sampling of terahertz beams," *Appl. Phys. Lett.*, vol. 67, no. 24, pp. 3523–3525, 1995.

[28] M. C. Nuss and J. Orenstein, "Terahertz time-domain spectroscopy," in *Millimeter and Submillimeter Wave Spectroscopy of Solids*. G. Grüner, Ed., Berlin, Germany: Springer, 1998.

[29] R. Dorn, S. Quabis, and G. Leuchs, "The focus of light—Linear polarization breaks the rotational symmetry of the focal spot," *J. Mod. Opt.*, vol. 50, no. 12, pp. 1917–1926, Aug. 2003.

[30] M. Born and E. Wolf, *Principles of Optics: Electromagnetic Theory of Propagation, Interference and Diffraction of Light*. Cambridge, U.K.: Cambridge Univ. Press, 1990.

[31] M. Yi, K. Lee, J.-D. Song, and J. Ahn, "Terahertz phase microscopy in the sub-wavelength regime," *Appl. Phys. Lett.*, vol. 100, no. 16, p. 161110, 2012.

Marco Peccianti received the M.Sc. degree (full marks and Hons.) in electronic engineering from the University of Rome "Roma Tre," Rome, Italy, in May 2000, and the Ph.D. degree from the Nonlinear Optics and Optoelectronics Lab, University of Rome "Roma TRE," in 2004.

In March 2007, he joined the Statistical Mechanics and Complexity group (SMC, Rome, Italy). He is currently a Permanent Researcher at the Institute for Complex Systems, Italian National Research Council (CNR), Rome, Italy. He is author of more than 140 contributions on scientific journals and conference proceedings on nonlinear photonics and THz optics with more than 2300 citations.

Dr. Peccianti received the "Best Young Physicist" prize "Vincenzo Caglioti" from the "Accademia Nazionale dei Lincei" in 2003 and the Otto Lehmann International Award from Karlsruhe University, Germany, in 2005.

Matteo Clerici received the Master and Ph.D. degrees in physics from Università degli Studi dell'Insubria, Como, Italy, in 2006 and 2010, respectively.

He is currently a Research Fellow and a Marie Curie Fellow at INRS-EMT, QC, Canada, and at Heriot-Watt University, Edinburgh, U.K. His research activities focus on intense terahertz and mid-infrared pulse generation, mainly from gas ionization and, more generally, on nonlinear optics in gasses and condensed media.

Alessia Pasquazi received the M.Sc. degree (full marks and Hons.) in electronic engineering from the University of Rome "Roma Tre," Rome, Italy, in July 2005, and the Ph.D. degree from the same university in spring 2009, where she was involved in investigating spatial solitons in liquid crystals, Kerr glasses, and nonlinear 2-D photonic lattices, as well as quadratic processes in waveguides and cubic effects in 3-D photonic crystals.

In April 2009, she received an Excellence Scholarship for Post-Doctoral research (MELS) from the Government of Quebec. She is currently a Postdoctoral Fellow at the INRS-EMT, QC, Canada. Her research interests include the theoretical and experimental investigation of nonlinear wave propagation in ultrafast quadratic and cubic materials, oriented to integrated devices.

Lucia Caspani received the Master and Ph.D. degrees in physics from Università degli Studi dell'Insubria, Como, Italy, in 2006 and 2010, respectively.

She is currently a MELS FQRNT Fellow at INRS-EMT, QC, Canada. Her research interests include generation of entangled states of light in integrated structures and numerical modeling of THz nonlinear interactions.

Sze Phing Ho received the B.Sc. degree in science (industrial physics) and the M.Sc. degree in science (physics) defending a thesis entitled "Properties of fabricated fiber Bragg gratings for temperature sensing using a phase mask technique" from the Universiti Teknologi Malaysia, Johor, Malaysia, in 2006 and 2008, respectively. Since May 2009, she has been working toward the Ph.D. degree in sciences and materials at the INRS-EMT, QC, Canada, where she is involved in a project focusing on THz imaging.

Fabrizio Buccheri received the B.E. and M.E. degrees in electrical engineering from the University of Palermo, Palermo, Italy, in 2007 and 2010, respectively. He is currently working toward the Ph.D. degree in optics under the supervision of Prof. X.-C. Zhang at the Institute of Optics, University of Rochester, NY.

After his graduation, he received a Fulbright scholarship in order to pursue a Ph.D. degree. His research interests include THz generation and detection schemes in gas plasma, with a particular focus to THz standoff detection.

Jalil Ali received the Ph.D. degree in plasma physics from Universiti Teknologi Malaysia (UTM), Johor, Malaysia, in 1990.

He is currently a Professor of Photonics at the Institute of Advanced Photonics Science, Nanotechnology Research Alliance and the Physics Department, UTM. Since 1987, he has held numerous faculty and research positions including that of Dean/Director, Bureau of Innovation and Consultancy. He was instrumental in establishing and forging University–Industry collaborations in Malaysia. He has authored/coauthored more than 300 technical papers published in international journal, three books, and a number of book chapters. His research interests include photonics, optical solitons, fiber couplers, and nanowaveguides. He is currently the Head of the Nanophotonics Research Group, UTM.

Dr. Ali is a member of the Optical Society of America, the International Society for Optical Engineers, and the Malaysian Institute of Physics.

Alessandro Busacca received the "Laurea" degree (full marks and Hons.) in electronics engineering from the University of Palermo, Palermo, Italy, in 1998, and the Ph.D. degree in 2001.

He was a Research Fellow at the Optoelectronics Research Centre, University of Southampton, Southampton, U.K., from 2000 to 2002. He became a Researcher at the University of Palermo in 2005, being tenured as a Permanent Faculty Member in 2008. Since November 2011 he is Associate Professor of "Electronics." His investigations include the design, fabrication, and characterization of optical devices, with specific interest for photonic microtechnologies, integrated and fiber optical devices. He is an author of more than 120 papers in journal and conference proceedings and of an international patent.

Dr. Busacca is a member of the Chapter Executive Committee in the IEEE Photonics Society. He is currently serving as a Reviewer of research proposals for the Italian Ministry of Research and the European Community.

Tsuneyuki Ozaki received the B.Sc., M.S., and Ph.D. degrees from the University of Tokyo, Tokyo, Japan, in 1987, 1989, and 1998, respectively.

From 1990 to 2000, he was a Research Associate at the Institute for Solid State Physics, University of Tokyo. From 2000 to 2003, he was a Research Specialist at Nippon Telegraph and Telephone Basic Research Laboratories, Atsugi, Japan. In 2003, he joined the INRS-EMT, University of Quebec, Varennes, QC, Canada, as an Assistant Professor, where he is currently a Full Professor and Director of the Advanced Laser Light Source. Since 2006, he has also been an Invited Researcher at the Research Centre, Maisonneuve-Rosemont Hospital, Université de Montréal, Montreal, QC. His main research interests include high-intensity THz radiation and their applications, intense high-order harmonic generation, and the application of lasers to medicine.

Dr. Ozaki is a member of the Optical Society of America and the International Society for Optical Engineers.

Roberto Morandotti received the M.Sc. degree in physics from the University of Genova, Genova, Italy, and the Ph.D. degree in electronics engineering from the University of Glasgow, Glasgow, U.K., in 1993 and 1999, respectively.

From 1999 to 2001, he was with the Weizmann Institute of Science, Rehovot, Israel. From 2002 to 2003, he was with the University of Toronto, ON, Canada, where he dealt with nonlinear discrete systems and the characterization of novel integrated optical structures, respectively. In June 2003, he joined the INRS-EMT, Varennes, QC, Canada, where he has been a Full Professor since 2008. He is the author and coauthor of more than 450 papers published in international scientific journals and conference proceedings. His current research interests include the linear and nonlinear properties of various structures for integrated optics, the study of novel technologies for optoelectronics applications as well as linear and nonlinear optics at unusual wavelengths (such as THz).

Dr. Morandotti is a Fellow, among others, of the Royal Society of Canada, of the Optical Society of America, and of the International Society for Optical Engineers. He has also served as a Technical Committee Member and Chair for several Optical Society of America, Laser and Electro-Optics Society, IEEE, and International Society for Optical Engineers meetings.